Expert Systems With Applications 115 (2019) 486–498

Contents lists available at ScienceDirect

Expert Systems With Applications

journal homepage: www.elsevier.com/locate/eswa

Ultrasound image segmentation using a novel multi-scale Gaussian kernel fuzzy clustering and multi-scale vector field convolution

Lipismita Panigrahi[a], Kesari Verma[a,*], Bikesh Kumar Singh[b]

[a] Department of Computer Applications, National Institute of Technology Raipur, C.G. 492010, India
[b] Department of Biomedical Engineering, National Institute of Technology Raipur, C.G. 492010, India

ARTICLE INFO

Article history:
Received 6 September 2017
Revised 4 August 2018
Accepted 10 August 2018
Available online 11 August 2018

Keywords:
Ultrasound image segmentation
Speckle reduction
Multi-scale Gaussian kernel induced fuzzy C-means
Multi-scale vector field convolution

ABSTRACT

Ultrasound imaging is most popular technique used for breast cancer screening. Lesion segmentation is challenging step in characterization of breast ultrasound (US) based Computer Aided Diagnosis (CAD) systems due to presence of speckle noise, shadowing effect etc. The aim of this study is to develop an automatic lesion segmentation technique in breast US with high accuracy even in presence of noises, artifacts and multiple lesions. This article presents a novel clustering method called Multi-scale Gaussian Kernel induced Fuzzy *C*-means (MsGKFCM) for segmentation of lesions in automatically extracted Region of Interest (ROI) in US to delimit the border of the mass. Further, a hybrid approach using MsGKFCM and Multi-scale Vector Field Convolution (MsVFC) is proposed to obtain an accurate lesion margin in breast US images. Initially, the images are filtered using speckle reducing anisotropic diffusion (SRAD) technique. Subsequently, MsGKFCM is applied on filtered images to segment the mass and detect an appropriate cluster center. The detected cluster center is further used by MsVFC to determine the accurate lesion margin. The proposed technique is evaluated on 127 US images using measures such as Jaccard Index, Dice similarity, Shape similarity, Hausdroff difference, Area difference, Accuracy, *F*-measure and analysis of variance (ANOVA) test. The empirical results suggest that the proposed approach can be used as an expert system to assist medical professionals by providing objective evidences in breast lesion detection. Results obtained are so far looking promising and effective in comparison to state-of-the-art algorithms.

1. Introduction

According to American Cancer Society's report, 2017, breast cancer is the second leading cause of death among adult females (Dora, Agrawal, Panda, & Abraham, 2017). Early detection and screening is the first crucial step towards treating breast cancer. It plays a key role in breast cancer diagnosis and treatment. Several imaging modalities have been used to assess soft segmentation of an ultrasound (US) image. It is a process of isolating the image into different regions or partitions, which have a special clinical meaning. Among all the medical images, US imaging is most common for the diagnosis from different imaging modalities due to its non invasive nature, low cost and ease of availability. However, due to the poor quality of images the accurate and automatic segmentation of the breast US images is still challenging, which needs further manual intercession. The Computer Aided Diagnosis (CAD) systems is emerged as an alternative tool for medical image analysis by offering several essential aids and more accuracy during clinical exploration even in the case limited performances apparatus (Joo, Yang, Moon, & Kim, 2004). However, the existing CAD systems are far away from their real time use due to their poor segmentation accuracy, specificity, sensitivity etc. An article Laursen (2016), states that computerized diagnosis aids do not yet measure up to the performance of human doctors and thus more study is required to evaluate the performance of CAD systems. A recent review by Cahan (2017) revealed the drawbacks and limitations of existing CAD systems. This review pointed that computerized diagnosis support systems are still not generally used by internists as such systems cannot efficiently recognize patterns and are unable to consider the base rate of potential diagnoses due to poor data quality and complex representation of data. The high complexity of designing an effective and viable system is reflected by the infrequent clinical use of such systems despite of serious efforts put in developing them. A recent study on ultrasound based CAD systems also highlight that the existing CAD systems suffers from several drawbacks due to restrictions posed by poor quality of images, size of image database and regulatory and commercial standards limiting their use in clinical practice

* Corresponding author.
E-mail addresses: lpanigrahi.phd2015.mca@nitrr.ac.in (L. Panigrahi), kverma.mca@nitrr.ac.in (K. Verma), bsingh.bme@nitrr.ac.in (B.K. Singh).

https://doi.org/10.1016/j.eswa.2018.08.013
0957-4174/

(Bikesh, 2017). The aim of this study is to develop an automatic lesion segmentation technique in US with high accuracy even in presence of noises, artifacts and multiple lesions. Several studies have been reported emphasizing the significance of accurate lesion segmentation in decision making process of CAD system. For example, a recent review on automated breast ultrasound image segmentation by Xian et al. (2018) and Min et al. (2017) states that, based on the results of segmentation, quantitative features such as tumor shape, size, echo pattern, etc., can be derived and supplied as input to a classifier to determine the category of the tumors. Therefore, the precision of breast ultrasound segmentation directly affects the decision making performance CAD systems. This article presents a novel clustering method called Multi-scale Gaussian Kernel induced Fuzzy *C*-means (MsGKFCM) for segmentation of lesions in automatically extracted Region of Interest (ROI) in US to delimit the border of the mass. Further, a hybrid approach using MsGKFCM and Multi-scale Vector Field Convolution (MsVFC) is proposed to obtain an accurate lesion margin in breast US images. Initially, the images are filtered using speckle reducing anisotropic diffusion (SRAD) technique. Subsequently, MsGKFCM is applied on filtered images to segment the mass and detect an appropriate cluster center. The detected cluster center is further used by MsVFC to determine the accurate lesion margin.

1.1. Related work

In past years, several algorithms have been reported in the literature for image segmentation. Fuzzy clustering is one of the popular technique (Gupta, Anand, & Tyagi, 2015; Kyung et al., 2014; Zhang, Huang, Li, Yang, & Wang, 2012) in which clusters are recognized via similarity measures. Lo et al. (2014) proposed watershed transform algorithm to group the related tissues around local minima to develop homogeneous regions, learning automata proposed by Sang, Lin, and Acton (2016) is used for iteratively calculating the Gaussian component parameter. Avendi, Kheradvar, and Jafarkhani (2016) proposed deep learning technique that automatically extract the features of the image and perform classification operation, Markov field anticipated by Gerard, Joan, Robert, Sergi, and Alison (2016) proposed a mean of integrating the divisions of image tissue classes as a spatial smoothness constraint and also presented a suitable means to model the relative information of the image, Self-Organizing Map (SOM) is used for magnetic resonance (MR) image segmentation proposed by Ortiz, Górriz, Ramirez, and Salas-Gonzalez (2011, 2012, 2014).

However, in literature various research work on the US image segmentation is deliberated along with active contour model (Gao, Wen, Wang, & Xu, 2017; Gupta et al., 2015; Li & Acton, 2007). The two main approaches of image segmentation through active contours are edge based (Chunming, Chenyang, Changfeng, & Fox, 2005, 2010) and region based (Chunming, Chiu-Yen, Gore, & Zhaohua, 2007; Rastgarpour, Shanbehzadeh, & Zadeh, 2014; Yuan, 2012, 2013). The edge based method of image segmentation is based on threshold or local filtering and region based segmentation is based on pixels which involves the selection of initial seed points to obtain the lesion (Chen, Yin, Flynn, & Broschat, 2003; Madabhushi & Metaxas, 2003; Panigrahi, Verma, & Singh, 2016). The edge based parametric active contour method is further extended such as balloon snake (Cohen, 1991; Cohen & Cohen, 1993), gradient vector flow snake (GVF) (Ray & Acton, 2004; Xu & Prince, 1997, 1998), vector field convolution (VFC) (Li & Acton, 2007) and MsVFC (Sassi, Sellami, Slima, Hamida, & Chtourou, 2014). In the entire active model, the desired features of images are captured by minimizing the energy function subject to certain constraints. The energy function contains two terms: an internal energy which constrains the efficiency and rigidity of the model, and an external energy, which attracts the flexible model to the features of interest (FOI) (Li & Acton, 2007).

Having reviewed the aforementioned studies, we observed that entire active model has been widely used, but there are certain limitations like, in GVF method (Li & Acton, 2007), the computation cost is high, noise sensitivity, parameter sensitivity and the relationship is ambiguous between the captured range and parameters. Sassi et al. (2014) reported that in VFC method, it is difficult to calculate the external force and the edge quality if the image is corrupted by noise. Sometimes ambiguous result may be obtained using different contour on the same image due to improper initialization of contour. Table 1 emphasise some of the recently reported techniques for breast US image segmentation based on the performance.

1.2. Contribution and organisation of the paper

We summarize the novelties and contributions of the paper as follows:

- Applied a speckle reducing anisotropic diffusion (SRAD) technique by building a multi-scale demonstration for each image where the noise is regularly reduced as the scale increases.
- Proposed a novel clustering algorithm called MsGKFCM. The objective function of the conventional GKFCM is modified for multi-scale thus the result from a coarse scale supervises the cluster of the next fine scale. The detail description of the segmentation technique described in Section 3.3.1.
- Proposed a novel hybrid approach by combining MsGKFCM and MsVFC technique in order to obtain an accurate lesion margin in breast US images described in Section 3.3.2.
- An extensive comparative investigation of the proposed method in light of state of the art methods is presented based on performance evaluation measures such as: Jaccard Index, Dice similarity, Shape similarity, Hausdroff difference, Area difference.

The rest of the paper is organized as follows. Section 2 presents the background of MsGKFCM clustering technique and MsVFC boundary detection techniques. Section 3 presents the material and methods used in the proposed approach. The experimental results is presented and discussed in Section 4 and finally, Section 5 concludes the paper.

2. Theoretical background

2.1. Clustering based segmentation techniques

In this section we discuss about different segmentation techniques which led to formulation of MsGKFCM. The brief preliminary notations are revealed in the Table 2. Let $X = \{x_1, x_2, \ldots, x_n\}$ is a data set in a two dimensional Euclidean space R^N with its norm $\|\cdot\|$ (Yang & Tsai, 2008). Let C be a positive integer representing number of clusters, where, $C > 1$. If X is divided into C parts then it can be represented as a disjoint set of $X_1, X_2, \ldots, X_c$ such that $X_1 \bigcup X_2 \bigcup \ldots \bigcup X_c = X$, or equivalently by the indicator functions $\mu_1 \ldots . \mu_c$ (where, $\mu_1 \ldots . \mu_c$ is known as a hard c-partition of clustering X into c such that $\mu_{ji} = \mu_j(x_i) = 1$ if $x_j \in X_j$ and $\mu_{ji} = 0$ if $x_i \notin X_j$ for i=1,...,n and j=1,...,c.

Ruspini (1969) first calculated an expansion to allow $\mu_{ji} = -\mu_j(x_i)$ being the membership functions of fuzzy sets μ_j on X and within the interval [0, 1] such that $\sum_j^c \mu_j(x_i) = 1$ for all x_i in X.

Dunn (1973) implanted the c-partitions into *K*-means and projected fuzzy *c*-means (FCM). Further, Bezdek (1981) enhanced FCM by replacing the weighting exponent m= 2 to any $m > 1$ and

Table 1
Benchmarking table.

Authors and Year	Data Sets (DS)	Technique	Performance (%)	Ground truth validation	Pros	Cons
Gerard et al. (2016)	33(14 Malignant and 19 benign)	Markov Random Field (MRF) and Maximum a Posteriori (MAP)		Yes	Integrate tissue stiffness information from ultrasound elastography, Organize breast US knowledge and image information in a unified framework and multiple-object segmentation	Assume the Gaussian distribution of features, Only obtain local optimal solution, Sensitive to initial parameter estimation and inefficient optimization algorithm. (Min et al., 2017)
Rogai, Manfredi, and Bocchi (2016)	Breast DS(275 images), Anesth Annulus DS (150 images), Anesth Vascular DS (80 images), Gyn Follicles DS (50 images)	Fuzzy logic, particle swarm optimization (PSO)	Specificity= 93.7(Breast DS), 93.9(Anesth Annulus DS), 90.1(Anesth Vascular DS), 91.7(Gyn Follicles DS)	Yes	Tackled the optimization problems.	-
Haoyang et al. (2015)	450 (213 benign and 237 malignant)	Saliency model	similarity ratio =73.74, Hausdroff error = 50.19, average mean absolute error = 13.44	Yes	–	-
Wang et al. (2014)	Synthetic images, 4 breast tumor and twenty liver ultrasound images.	Multi scale geodesic active contour (GAC).	JI=97.33	No	Exploited the geometric information between different scales and also does not suffers the weakness inherent with Gaussian smoothing.	Cannot adapt to segment multiple tumors and sensitive to initialization.
Lo et al. (2014)	68 benign and 65 malignant tumors.	Watershed transform and 2-D/3- D False Reduction.	Sensitivity of Positive 100% With 9.44 FPs/ pass.	Yes	Less operator dependent, greater reproducibility, accelerate the reviewing procedure and reduce oversight errors.	Depended on image enhancement and needed additional geometrical measure to decide the final tumor contour. Min et al. (2017)
Kyung et al. (2014)	148 (68 benign and 80 malignant)	Fuzzy c-means	Sensitivity = 89.19	Yes	High sensitive rate, each data point can belong to every cluster with a corresponding membership value rather than just belongs to one cluster as in *K*-means.	Can not deal with the blur boundary and uncertainty in breast US images. Min et al. (2017)
Gerard, Robert, Sergi, Melcior, and Joan (2014)	163 (54 malignant and 109 benign)	Deformable part models (DPM)	Sensitivity = 86	No	Reduce Sensitivity.	Cannot adapt to segment multiple tumors. Min et al. (2017)
Bo et al. (2010)	79(33 benign and 46 malignant)	Active contour, level set	Similarity index = 88.07, williams index = 0.8656, Pearson's correlation coefficient = 0.9241	Yes	Model the difference between the estimated prior distribution and the regional intensity distribution.	Slow, sensitive to initialization. Min et al. (2017)
Juan et al. (2012)	122(58 benign and 64 malignant)	Neutrosophic l-means(NLM)	Similarity index = 86.3 ± 5.5, Hausdorff distance (pixel) = 22.5 ± 12.9, mean absolute distance (pixel) = 4.8 ± 2.4	Yes	Deal with indeterminate regions effectively and accurately, it can smooth the complex background.	It is very sensitive to noise therefore cannot deal effectively with uncertainties and gives wrong output for blurred and noisy breast US images containing shadow effects Lal, Kaur, and Gupta (2017).

defined a modified FCM described in Eq. (1).

$$J_m(\mu, a) = \sum_{i=1}^{n}\sum_{j=1}^{c} \mu_{ji}^{m}\|x_i - a_j\|^2 \quad (1)$$

Although FCM have the capability to solve the doubtful cases, but it has certain limitations (Ahmed, Yamany, Mohamed, Farag, & Moriarty, 2002):

1. The cluster results are always affected by outliers.
2. The segmentation accuracy is affected as it is very sensitive to noise (Gupta et al., 2015).
3. The spatial information in image space are not considered.

To overcome these limitations (Ahmed et al., 2002) introduced a bias-corrected FCM (BCFCM). Furthermore, Chen and Zhang (2004) found a drawback in BCFCM that computing the neighborhood terms R_i consume more time than FCM and proposed a customized objective function J_m^{cz}. Later on, in order to increase the performance of clustering results, Chen and Zhang (2004) replaced the Euclidean distance $\|x_i - a_i\|^2$ with a Gaussian kernel induced distance $\|\phi(x_i) - \phi(a_j)\|^2$ by the kernel substitution (defined in Eq. (2)) to construct the kernel version of

Table 2
Preliminary notations.

Symbol	Description
α	Scaling factor
β	Scaling factor
τ=0.5	Constant
μ=0.2	Constant
$m = 2$	Weighted exponent
N=3	Number of cluster
U	Objective function
a	Centroid
u	Membership function
t	Time stamps

the FCM. Further the objective function of FCM modified as J_m^K.

$$\|\phi(x_i) - \phi(a_j)\|^2 = K(x_i, x_i) + K(a_j, a_j) - 2K(x_i, a_j) \tag{2}$$

where, ϕ is a nonlinear transformation from the data space into the feature space with its equivalent kernel K. They assumed $K(x, y) = 1$ and anticipated the kernel-type objective function J_m^K. An advantage of J_m^K is that, the clustering is performed still in the original place and thus the results can be easily intuited. However, according to Ahmed et al. (2002) FCM only take care of pixel intensity and does not contain the spatial information in image space. To avoid this limitation, Chen and Zhang (2004) replaced the Euclidean distance $\|x_i - a_j\|^2$ with a Gaussian kernel induced distance $1 - K(x_i - a_j) = 1 - exp(-\|x_i - a_j\|/\sigma^2)$ to construct the GK-FCM with spatial constraints. Subsequently the objective function J_m^K is modified as JS_m^K described in Eq. (3) and the necessary conditions for minimizing JS_m^K are described in Eqs. (4)–(5).

$$JS_m^K(\mu, a) = \sum_{i=1}^{n}\sum_{j=1}^{c}\mu_{ji}^m(1 - K(x_i, a_j)) + \alpha\sum_{i=1}^{n}\sum_{j=1}^{c}\mu_{ji}^m(1 - K(\bar{x}_i, a_j)) \tag{3}$$

where,

$$a_j = \frac{\sum_{i=1}^{n}\mu_{ji}^m(K(x_i, a_j)x_i + \alpha K(\bar{x}_i, a_j)\bar{x}_i)}{\sum_{i=1}^{n}\mu_{ji}^m K(x_i, a_j) + \alpha K(\bar{x}_i, a_j)} \tag{4}$$

$$\mu_{ji} = \frac{((1 - K(x_i, a_j)) + \alpha(1 - K(\bar{x}_i, a_j)))^{\frac{-1}{m-1}}}{\sum_{k=1}^{c}((1 - K(x_i, a_k)) + \alpha(1 - K(\bar{x}_i, a_k)))^{\frac{-1}{m-1}}} \tag{5}$$

Wang and Fei (2009) proposed a modified FCM called multi-scale fuzzy *C*-means (MsFCM) to improve the classification speed and avoid trapping into local solutions. The multi-scale approach has been demonstrated as an efficient technique to reduce the computational cost and the risk of converging to local minima. In this approach global information is extracted and maintained in large scale (coarse scales) and low-scale (fine scale) images contains the detailed local information. The modified objective function for MsFCM is described in Eq. (6).

$$J_m^{MsFCM}(\mu, a) = \sum_{i=1}^{n}\sum_{j=1}^{c}\mu_{ji}^m\|x_i - a_j\|^2 + \frac{\alpha}{R_N}\sum_{i=1}^{n}\sum_{j=1}^{c}\mu_{ji}^m\sum_{x_r\in R_i}\|x_r - a_j\|^2 + \beta\sum_{i=1}^{n}\sum_{j=1}^{c}(\mu_{ji} - \mu'_{ji})^m\|x_i - a_j\|^2 \tag{6}$$

2.2. Boundary detection techniques

This section elaborates contour detection techniques used in this study.

2.2.1. Parametric active contours

A traditional active contour snake is signified by a parametric curve that deform through the image domain and try to shift the boundary in such a position where its energy is minimized. Kass, Witkin, and Terzopoulos (1988) proposed an energy function for calculating the contour energy that is defined in Eq. (7).

$$E(C) = \int_0^1 [E_{insidec}(V(s)) + E_{outsidec}(V(s))] \tag{7}$$

In Eq. (7) the energy function is divided into two parts. The first part $E_{insidec}$ defined in Eq. (8) (Li & Acton, 2007).

$$E_{insidec} = \frac{1}{2}(\alpha|V'(s)|^2) + \beta|V''(s)|^2 \tag{8}$$

where, α and β are weighting parameter that represent the contour's efficiency and tautness respectively, whereas $|V'(s)|$ and $|V''(s)|$ represent the first and second derivative of $V(s)$ with respect to s.

The second part $E_{outsidec}$ defined in Eq. (9) represents the external energy derived from the image (Li & Acton, 2007).

$$E_{outsidec}(x, y) = -|\nabla I(x, y)|^2 \tag{9}$$

When the contour needs to minimize its overall energy, different calculus techniques are used to minimize the energy function defined in Eq. (7), which satisfy Euler–Lagrange equation defined in Eq. (10).

$$\alpha V''(s) - \beta V''''(s) - \nabla E_{outsidec}(V(s)) = 0 \tag{10}$$

This can be considered as a force balance equation defined in Eq. (11).

$$F_{insidec}(V) + F_{outsidec}(V) = 0 \tag{11}$$

In this respect there are three terms in Eq. (10), the first two terms are corresponding to the $F_{insidec}$ and the third term is treated as $F_{outsidec}$.

To solve Eq. (9),$V(s)$ is treated as a function of time. The solution is obtained when the steady state solution of the following gradient descent Eq. (12) is reached from an initial contour $V(s,0)$.

$$\frac{\partial v(s,t)}{\partial t} = \alpha V''(s,t) - \beta V''''(s,t) + F_{outsidec}(V(s,t)) \tag{12}$$

2.2.2. Vector field convolution

Li and Acton (2007) introduced a static external force called VFC. The aim of this study is to find the external force field, given an edge map when the edge derived from the image is corrupted by noise. This external force is calculated by convolving a specific vector field kernel with the edge map. The VFC external force is defined in Eq. (13).

$$F_{vfc}(x, y) = f(x, y) * k(x, y) \tag{13}$$

where, $f(x,y)$ is the edge map derived from image, $k(x,y)$ is the vector field kernel in which all vector points to the kernel origin is written in Eq. (14).

$$k(x, y) = m(x, y)n(x, y) \tag{14}$$

where, $m(x,y)$ is the magnitude of the vector at (x,y) and $n(x,y)$ is the unit vector pointing to the kernel origin (0,0), m and$n$ are defined in Eqs. (15)–(17).

$$n(x, y) = \left[-x/r, -y/r\right] \tag{15}$$

$$m_1(x, y) = (r + \varepsilon)^{-\gamma} \tag{16}$$

Or,

$$m_2(x, y) = exp\left(-\frac{r^2}{\zeta^2}\right) \tag{17}$$

where, the radius $r = \sqrt{x^2 + y^2}$, m_1 is a decreasing function of r, which typically employs $\gamma = 2$ and ε as a small constant that prevents division by 0 at the origin and m_2 is a Gaussian decay with width given by the standard deviation ζ. m_1 and m_2 are also isotropic, resulting in that diffusion of image forces is identical in all directions. The series of a VFC force field is specified by the convolution kernel width. In m_1 the width is identified by radius r, and in m_2, it is managed by ζ.

2.2.3. Multi-scale vector field convolution

Though VFC illustrates resilience to efficiency, noise and extended capture range but it has certain limitations, which are inherent to convolution.

- In the convolution that produces VFC, force vectors are subject to cancellation or directional bias depending on place and size of the kernel (Yang & Acton, 2012).
- If noise is present in the image, it might prevent the snake from correctly finding the contours of an object and thus, the resultant object's contour may be closer by the initial snake curve than otherwise (Sassi et al., 2014).

To overcome this limitations, Yang and Acton (2012) proposed MsVFC which is the extended version of VFC. MsVFC convolves an image edge map $f(x, y)$ with a bank of vector kernels over a range of scales t defined in Eq. (18)

$$F_{MsVFC}(x, y; t) = f(x, y) * [m_{norm}(x, y; t) \cdot n(x, y)] \tag{18}$$

where, $t \epsilon [t_{\min}, t_{\max}]$, the force range of a MsVFC field is set by the width of the largest VFC kernel organized in the MsVFC filter set, which is $t_{\max}$. The minimum resolution MsVFC is imposed by $t_{\min}$, that directly attributes to a degree in detail preservation of MsVFC forces. The magnitude function m_1 (Power-decay) and m_2 (Gaussian-decay) are defined in Eqs. (19)–(20).

$$m_{1,norm}(x, y; t) = \frac{(r + \varepsilon)^{-1}}{2\pi t - \pi r_0} \tag{19}$$

$$m_{2,norm}(x, y; t) = \frac{exp(-r^2/t^2)}{2t^2} \tag{20}$$

where, Eq. (19) is calculated for a peculiar case where the power $\gamma = 1$. Scale (t) is defined as the standard deviation of the Gaussian ζ. The function is truncated at a small radius r_0 in order to approximate the total volume underneath because m_1 approaches $+\infty$ at location (0,0). Normalization is required so that external forces produced at the same pixel position, merely at different scales can be compared on equal basis.

Another major drawback of VFC method (Sassi et al., 2014) is that the selection of the Gaussian smooth operator ζ is strict and the contour extracted by fixed ζ is not accurate for all images. For higher value of ζ, the features of the image may be blurred simultaneously for lower value of ζ, the curve becomes more smoothen. To overcome this problem (Sassi et al., 2014) proposed MsVFC with different value of ζ. For optimal value of ζ, it smoothen the image and snake exceed the noise conforming the accurate detection of shape. The stopping condition has been evaluated using Eq. (21) and the equation will be iterated continuously till the stopping condition not satisfied.

$$\frac{\left\| v(s)^t - v(s)^{t-1} \right\|}{n} < S \tag{21}$$

where, $v(s)^t$ and $v(s)^{t-1}$ are vectors containing the indices of the snake points at time step t and t-1 respectively, S is a small threshold and n the total number of snake points.

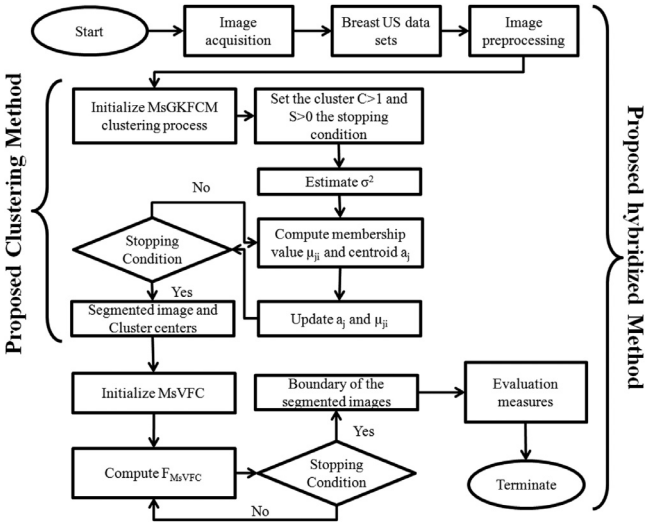

Fig. 1. Flow chart of the implementation structure.

2.3. Origin of the problem

Though GKFCM, MsFCM and MsVFC are the benchmarking methods, However it suffer from following limitations.

1. GKFCM described in Eq. (3) does not update the membership of each pixel in a coarse-to-fine manner (Wang & Fei, 2009).
2. In MsFCM the level in the data sets is thought as evenly important. It considers the number of degrees in the cluster is almost equal and all the points can not have a membership value of one (Yang & Tsai, 2008).
3. The objective function used in MsFCM described in Eq. (6) increase the computational time for cluster creation (Chen & Zhang, 2004).
4. MsVFC method is sensitive to center initialization (Min et al., 2017).

To overcome these limitations, we propose a novel clustering technique called MsGKFCM and develop a hybrid boundary detection technique described in Section 3.3.

3. Material and methods

The block diagram of the proposed technique is depicted in the Fig. 1. The first step is to applying SRAD filter to reduce speckle noise in breast US images by building a multi-scale representation for each input image where the noise is regularly reduced as the scale increases. The boundaries at coarse scales are highly preserved due to the edge sensitive property of the SRAD filter. The next step is, to segment the filtered mass by utilizing MsGKFCM and find the appropriate cluster center to initialize MsVFC, the third step is applying the MsVFC to find out the boundary. The MATLAB R2015a and Dev C++ software is used to implement the SRAD filter (Yu & Acton, 2002), MsGKFCM and MsVFC. The various steps are explained as follows.

3.1. Demographics and data acquisition

The approval of Institutional Ethical Committee was granted to carry out this study protocol. In this study a total of 127 ultrasound B-scan images (75 malignant mass and 52 are solid benign mass) are used. The images are collected from Dr. Bhimrao Ambedkar Memorial Hospital, Raipur, Chhatisgarh, India. Patient's identity was not disclosed and their informed consent was taken. The

Table 3
Demographic of data.

Parameter	Value
Total Number of images	127
Number of malignant masses	75
Number of benign masses	52
Age	16–70
Geographical locations	Chhattisgarh, Odisha, Maharashtra region (India)
Type	True color
Resolution	256x256, with 90 dpi horizontal and vertical
US machine model	Samsung-RS80A
Frequency	89 Hz
Mechanical index (MI)	0.68
Thermal Index (TI)	0.2

breast ultrasound examination has been performed by the radiologist. The biopsy test of the suspicious tissue has been used for confirmation. The demographics of the studied subjects are summarized in Table 3.

The images that are collected for this study are true color images in Joint Photographic Expert Group (JPEG) format. The true color images were converted into 256 gray levels. The acquired ultrasound images were of variable sizes. Thus, a ROI is manually extracted to simplify the overall appearance of the image according to the guidelines of expert Radiologists. The size of ROI in mm is 72 mm $\times$ 72 mm.

3.2. Data preprocessing

US images based on different types of breast conditions, including both benign (non-cancerous) and malignant (cancerous) lesions and validated by experts. As US images are sensitive to noise the image filtering techniques help to improve the performance of segmentation. Conventional MsFCM uses anisotropic diffusion or bilateral filtering (Wang & Fei, 2009) to get multi-scale images. These filtering methods perform well for Magnetic resonance (MR) images, but not robust for US images that are corrupted by speckle noise (Zhang et al., 2012). To avoid this limitation, (Wang et al., 2014; Zhang et al., 2012) used SRAD filter to suppress speckle noise and smooth the US images at various scales and construct a multi-scale image series. Given an intensity image $I_i(x, y)$, the output image $I_o(x, y; t)$ of SRAD is evolving according to the Eq. (22).

$$\begin{cases} \partial(x, y; t)/\partial t = div[c(q)\nabla I_o(x, y; t)] \\ I_o(x, y; t) = I_i(x, y) \end{cases} \tag{22}$$

where, $c(q)$ is the diffusion coefficient defined in Eq. (23), there are two function in Eq. (23), the first one is the diffusion threshold $q_0(t)$ and the second function $q(x, y; t)$ is the instantaneous coefficient of variation, t is the diffusion time, which is described as $t = l \cdot n_t \cdot \Delta t$, where $l = 1, 2, \ldots, L$ is the scale, $l \cdot n_t$ is the number of iteration, n_t is the iteration interval, and Δt is the time step. Here, scale $l = 1$ is the finest scale, and scale $l = L$ is the coarsest scale. In this study, we set the number of scales $L = 8$ and iteration interval $n_t = 10$.

$$c(q) = \frac{1}{1 + [q^2(x, y; t) - q_0^2](t)/[q_0^2](t)(1 + q_0^2](t))} \tag{23}$$

SRAD not only suppresses speckle noise in breast US images, but also conserves edges and even enhances edges scale by scale while inhibiting diffusion across edges and allowing diffusion on either side of the edge.

3.3. Proposed method

The proposed objective function $J_m^{MsGKFCM}$ is derived from the objective function JS_m^K and J_m^{MsFCM}. However, the traditional GKFCM, MsFCM and MsVFC method have several limitations which is described in Section 2.3. The mentioned limitations can be solved using the proposed method as follows:

1. Aiming at the first shortcoming, the proposed method update the membership of each pixel in a coarse-to-fine fashion. i.e. The objective function of the conventional GKFCM method is modified by the Eq. (6) to allow multi-scale clustering process where the result from a coarse scale supervises the cluster of the next fine scale. The aim of using multi-scale approach is, to reduce the computational cost, improve the clustering speed and avoid trapping into local solutions.
2. In order to overcome the second limitation, the proposed approach use Gaussian kernel distance in place of Euclidean distance in the objective function of MsFCM. So that it can contain the spatial information in image space, the cluster results are not affected by outliers and the segmentation accuracy is improved.
3. To overcome the third limitation, the proposed approach replace the term $\frac{1}{R_N}\sum_{x_r \in R_i}\|x_r - a_j\|^2$ of Eq. (6) with $\|\bar{x}_i - a_j\|^2$ (Note: the term $\frac{1}{R_N}\sum_{x_r \in R_i}\|x_r - a_j\|^2$ in MsFCM can be consistently written as $\frac{1}{R_N}\sum_{x_r \in R_i}\|x_r - \bar{x}_i\|^2 + \|\bar{x}_i - a_j\|^2$. Thus the computation time for creating cluster can be saved when $\frac{1}{R_N}\sum_{x_r \in R_i}\|x_r - a_j\|^2$ in Eq. (6) is replaced with $\|\bar{x}_i - a_j\|^2$) (Chen & Zhang, 2004). Which is second part of the proposed approach.
4. In order to overcome the fourth limitation, the proposed approach initialize the MsVFC method by the result obtained from MsGKFCM method (i.e. the cluster center) to get the accurate lesion margin.

3.3.1. Proposed clustering method

The scale space in MsGKFCM is composed of series of images after filtering at various scales. The objective function of $J_m^{MsGKFCM}$ at a scale l (l = 1, 2, ..., L) and the necessary conditions for minimizing $J_m^{MsGKFCM}$ is defined in Eqs. (24)–(29).

$$\begin{aligned} J_m^{MsGKFCM} = & \sum_{i=1}^{n}\sum_{j=1}^{c}\mu_{ji}^m\left(1 - K\left(x_i, a_j\right)\right) \\ & + \alpha\sum_{i=1}^{n}\sum_{j=1}^{c}\mu_{ji}^m\left(1 - K\left(\bar{x}_i, a_j\right)\right) \\ & + \beta\sum_{i=1}^{n}\sum_{j=1}^{c}\left(\mu_{ji} - \mu'_{ji}\right)^m\left(1 - K\left(x_i, a_j\right)\right) \end{aligned} \tag{24}$$

The membership function is focused to the constraints that are defined in Eq. (24).

$$\sum_{j=1}^{c}\mu_{ji} = 1, \mu_{ji} \in [0, 1], \sum_{i=1}^{n}\mu_{ji} > 0 \tag{25}$$

where,

$$K(x_i, a_j) = exp\left(\frac{-\|x_i - a_j\|}{\sigma^2}\right) \tag{26}$$

$$\sigma^2 = \frac{1}{n}\sum_{i=1}^{n}\left\|x_i - \left(\frac{1}{n}\sum_{i=1}^{n} x_i\right)\right\|^2 \tag{27}$$

where,

$$a_j = \frac{\sum_{i=1}^{n}\mu_{ji}^{m}\left(K\left(x_i, a_j\right)x_i + \alpha K\left(\bar{x}_i, a_j\right)\bar{x}_i + \beta K\left(x_i, a_j\right)x_i\right)}{\sum_{i=1}^{n}\mu_{ji}^{m}\left(K\left(x_i, a_j\right) + \alpha K\left(\bar{x}_i, a_j\right) + \beta K\left(x_i, a_j\right)\right)} \tag{28}$$

$$\mu_{ji} = \frac{\left(\left(1 - K\left(x_i, a_j\right)\right) + \alpha\left(1 - K\left(\bar{x}_i, a_j\right)\right) + \beta\left(1 - K\left(x_i, a_j\right)\right)\right)^{\frac{-1}{m-1}}}{\sum_{k=1}^{c}\left(\left(1 - K\left(x_i, a_k\right)\right) + \alpha\left(1 - K\left(\bar{x}_i, a_k\right)\right) + \beta\left(1 - K(x_i, a_k)\right)\right)^{\frac{-1}{m-1}}} \tag{29}$$

where, μ_{ji} is the membership function of the pixel i in the j^{th} cluster, μ'_{ji} is the membership function at previous scale, x_i is the feature vector of the pixel i, a_j is the vector of the center of the class j cluster, m be the weighted exponent, α and β are the scaling factor. The part I of the Eq. (24) is the objective function of the traditional GKFCM method, in which high membership values are assigned to those pixels whose intensity values are closer to the center of the class. To regulate the clustering toward piecewise homogeneous group the part II of Eq. (24) allows the membership in the neighboring pixels. The part III incorporates the direction of information from the cluster of the preceding scale, μ'_{ji} is determined in Eq. (30) and adjusted by using a threshold s that is set as 0.85 in our study.

$$\mu'_{ji} = \begin{cases} \mu'_{ji}, if & \max\limits_{i}\{\mu'_{ji}\} > S \\ 0, & otherwise \end{cases} \tag{30}$$

After introducing MsGKFCM, we combine both the features of MsGKFCM and MsVFC to initialize the contour and to get an accurate lesion margin in breast US images. The detail description of MsVFC is described in Section 2.2.3.

3.3.2. Proposed hybridization algorithm

In the proposed hybridization method, the MsGKFCM clustering method driven by the MsVFC is used to obtain an accurate lesion margin in breast US images. For the purpose of initial segmentation the proposed method starts with the MsGKFCM clustering. Subsequently, the result of the MsGKFCM is used to initialize the MsVFC method. Automated segmentation of the breast US images and it's implementation in the above aspects is formulated in Algorithm 1.

Algorithm 1 Proposed hybridization algorithm.

Input

1: $I = \{i_1, i_2, \ldots i_n\}$, $i_i \in R^N$; //The breast US data set.
2: Initialize C, $C > 1$; //The number of clusters.
3: Initialize S, $S > 0$; //The stopping criterion of the algorithm.
4: Initialize m, $m > 1$; //Fuzzy exponent.
5: $a^{(0)} = (a_1^{(0)}, \ldots, a_C^{(0)})$; //The initial of cluster centers.
6: Set the scale $l = L$.

Output

1: Segmented Image.

Algorithm

1: Generate multi-scale images using SRAD.
2: Apply the MsGKFCM clustering algorithm on the filtered image.
3: Let N=1 and estimate σ^2 by using Eq. (27).
4:
5: Compute $\mu^{(N)}$ with $a^{(N-1)}$ by using Eq. (29).
6:
7: Update $a^{(N)}$ with $a^{(N-1)}$ and $\mu^{(N)}$ by using Eq. (28).
8:
9: **if** $\|a^{(N)} - a^{(N-1)}\| < S$ **then**
10: STOP and OUTPUT;
11: **else**
12: $S = S + 1$ and return step 4;
13: **end if**
14: Set the region of interest in the results of the MsGKFCM obtained from the step 1 and initialize the MsVFC by using step 14.
15: $F_{MsVFC}(x, y; t) = f(x, y) * [m_{norm}(x, y; t) \cdot n(x, y)]$ //$m_{1,norm}(x, y; t) = \frac{(r+\varepsilon)^{-1}}{2\pi t - \pi r_0}$ and $m_{2,norm}(x, y; t) = \frac{exp(-r^2/t^2)}{2t^2}$
16: **if** $\frac{\left\|v(s)^t - v(s)^{t-1}\right\|}{n} < S$ **then**
17: STOP and OUTPUT;
18: **else**
19: Return step 13;
20: **end if**

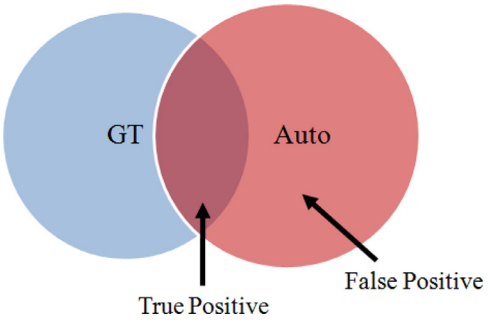

Fig. 2. Area corresponding to TP, FP regions.

3.4. Performance measures

The quantitative and qualitative evaluation of the performance of state of the art methods and the proposed method is carried out using the following measures, such as: the false positive (FP), the true positive (TP) (Fenster & Chiu, 2005; Gupta et al., 2015), true negative (TN) and false negative (FN) are applied.

If S_{GT}, S_{Auto} and T indicates the binary mask of segmented ground truth region, the automated segmented region and the pixels of the total image correspondingly then the TP represents number of pixels that are present in the ground truth segmented region (generated manually) as well as in automated segmentation technique. The FP represents number of pixels that are not present in the ground truth segmented region but present in automatically generated segmented lesion. The TP, FP, TN, FN are defined in Eqs. (31)–(34) and the area corresponding to TP, FP regions are shown in Fig. 2.

$$TP = \left|S_{GT} \cap S_{Auto}\right| \tag{31}$$

$$FP = \left|S_{GT} \cup S_{Auto} - S_{GT}\right| \tag{32}$$

$$FN = \left|S_{GT} \cup S_{Auto} - S_{Auto}\right| \tag{33}$$

$$TN = T - \left|S_{GT} \cup S_{Auto}\right| \tag{34}$$

With these measures, the different performance metrics that are used to access the performance of clustering and boundary detection methods are described in Eqs. (35)–(43).

a. *Accuracy* Accuracy (ACC) (Fenster & Chiu, 2005).

$$ACC = \frac{TP + TN}{TP + TN + FP + FN} \tag{35}$$

$$TPR/Sensitivity/Recall = \frac{TP}{TP + FN} \tag{36}$$

$$TNR/Specificity = \frac{TN}{TN + FP} \tag{37}$$

$$PPV/Precision = \frac{TP}{TP + FP} \tag{38}$$

$$F - Score = \frac{2 \times precision \times recall}{TP + FN + TN + FP} \tag{39}$$

b. *Jacard Index* Jaccard index (JI) (Udupa et al., 2002).

$$JI = \frac{\left|S_{GT} \cap S_{Auto}\right|}{\left|S_{Auto}\right| + \left|S_{GT}\right| - \left|S_{GT} \cap S_{Auto}\right|} \tag{40}$$

c. *Dice similarity* Dice similarity (DC) (Wang & Fei, 2009).

$$DS = 2 \times \frac{\left|S_{GT} \cap S_{Auto}\right|}{\left|S_{Auto}\right| + \left|S_{GT}\right|} \tag{41}$$

d. *Hausdorff distance* Hausdorff distance (HD) (Gupta et al., 2015).

$$HD(X, Y) = max\left\{sup_{x \in X} inf_{y \in Y} d(x, y), sup_{y \in Y} inf_{x \in X} d(x, y)\right\} \tag{42}$$

e. *Area difference* Area difference (AD) (Selvan, Kavitha, Shenbagadevi, & Suresh, 2010).

$$AD = \left(\frac{A_{GT} - A_{Auto}}{A_{GT}}\right) \times 100 \tag{43}$$

4. Results and discussions

This section presents the results of proposed approach and comparative evaluation of different clustering and contour detection methods. To evaluate the performance of the proposed method, exhaustive experiments have been conducted and the results were compared with state-of-the-art segmentation and boundary detection methods. The experiments were evaluated on 127 breast US images, however the result of 5 images (Figs. 3–5) are shown in this paper to illustrates the effectiveness of proposed approach. The comparison of the proposed method with the following state-of-the art techniques is presented in this paper.

Method 1: The *K*-means (Dunn, 1973).
Method 2: FCM algorithm (Dunn, 1973).
Method 3: The GKFCM algorithm (Yang & Tsai, 2008).
Method 4: The NLM clustering method (Juan, HD, & Yuxuan, 2012).
Method 5: **The proposed clustering known as MsGKFCM.**
Method 6: Graph-based method (Gerard et al., 2016).
Method 7: The watershed algorithm (Lo et al., 2014).
Method 8: **The proposed MsGKFCM technique based on MsVFC model.**

4.1. Segmentation and boundary detection results

In this research, a record of 127 breast US images were obtained to investigate the performance of the proposed method. After removing speckle noise from breast US images using SRAD filter MsGKFCM technique is used to segment the US images and search the efficient cluster center to initialize MsVFC. The results of various steps are shown in Fig. 3, that consists 5 samples, the first two are critical cases images and the rest 3 are simple case images. The original breast US images are illustrated in Fig. 3(a) and its manually described regions (filled with green), that is ground truth, generated by an expert are shown in Fig. 3(b) and (c) shows the results obtained from *K*-means, Fig. 3(d) shows the result obtained from FCM algorithm, Fig. 3(e) illustrates the result achieved from GKFCM algorithm, Fig. 3(f) represents the result obtained from NLM clustering, the result achieved from proposed technique MSGKFCM are illustrated in Fig. 3(g), the result achieved from Graph based method are shown in Fig. 3(h), the result achieved from Watershed algorithm are shown in Fig. 3(i) and (j) represents the results obtained from proposed MsGKFCM based on MsVFC model. The experimental results demonstrate that the proposed method not only segment the simple images, but also the critical cases more accurately. The segmentation outcomes achieved by the proposed method are very closed to the manually described ground truth region in most of the cases.

4.2. Quantitative evaluation

This section presents quantitative results of the proposed segmentation and boundary detection approaches. Further, we compared the results of proposed method with the state of art segmentation and boundary detection methods. The corresponding quantitative outcomes are summarized in Table 4–8, which shows the performance measures such as the TP, FP,TN, FN, ACC, HD, JI and DS for all breast US images.

Table 4 shows the performance of different segmentation methods with respect to JI, DS and AD. It can be observed that the value of JI and DS is highest for the proposed method and achieves lowest AD values as compared to other state of the art methods due to GKFCM is applied along with multiple scales for construction of crude image to fine. The aim of using multi-scale approach is to reduce the computational cost, improve the clustering speed and avoid trapping into local solutions. We found that the JI and DS obtained by the proposed method assures more similarity between the regions extracted by the ground truth and automated segmentation method.

Table 5 presents HD obtained for five breast US images when different boundary detection techniques are applied. It is found that the proposed method achieves lowest HD as compared to other boundary detection methods due to multi-scale SRAD filter has the capability to reduce speckle noise, as a result the noise is regularly reduced as the scale increases but the boundaries at coarse scales are still preserved due to the edge sensitive property. Therefore, when the proposed approach is applied on filtered mass, it gets appropriate cluster center to overcome the initialization problem of MsVFC.

Table 6 presents the performance of different segmentation techniques in terms of accuracy. It is observed that the accuracy of proposed method is improved by 12.7978%, 7.8643%, 1.7358%, 15.0848%, 7.5318% and 37.1488% in compared to *K*-Means, FCM, GKFCM, NLM, Graph-based and watershed methods respectively. This study obtained higher accuracy due to it uses Gaussian kernel distance in place of Euclidean distance in the objective function of MsFCM (Euclidean distance is well on segmenting most noise-free images but it fails to segment the images corrupted by outliers and other imaging artifacts (Chen & Zhang, 2004)).

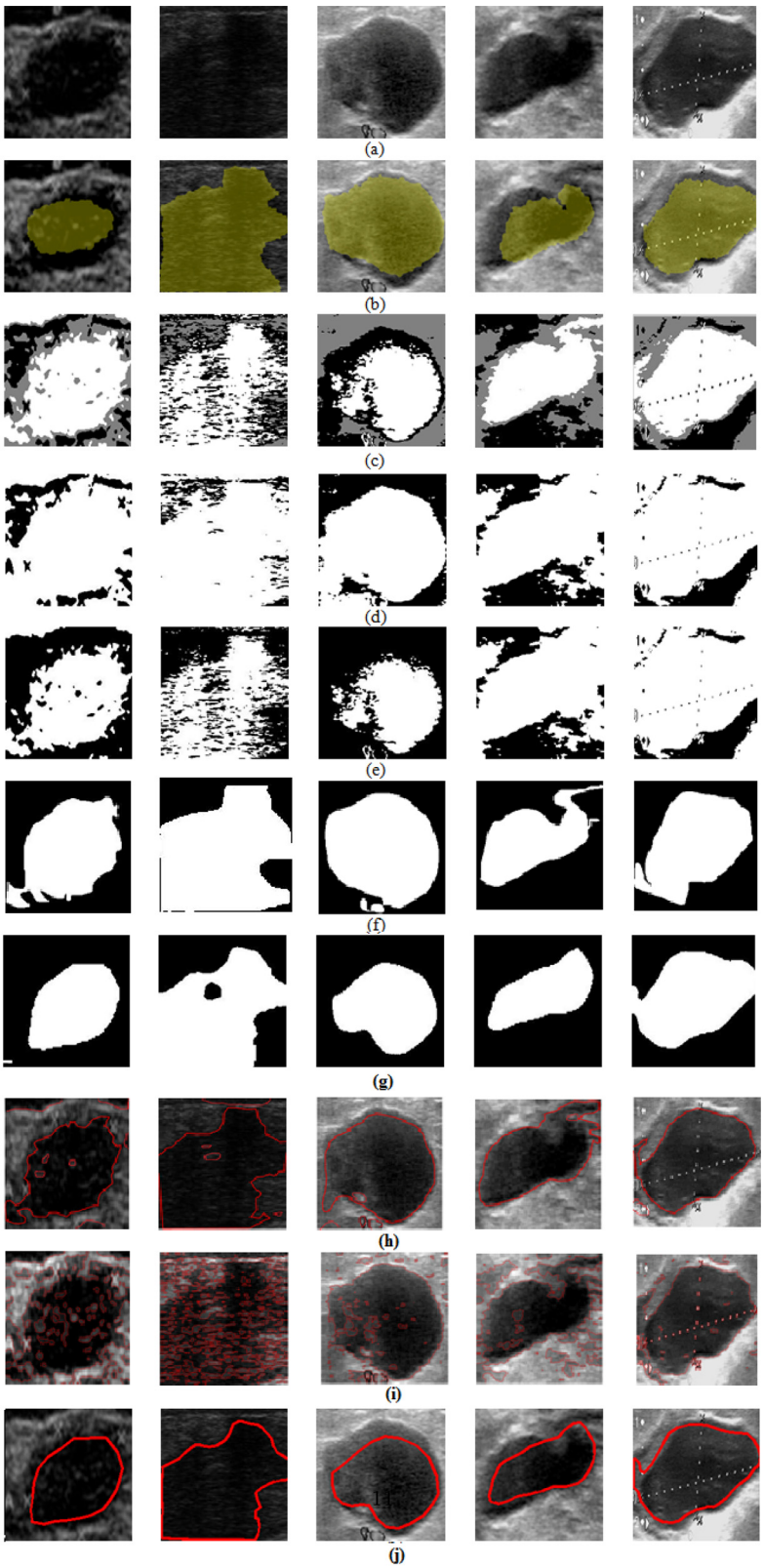

Fig. 3. (a) Original ultrasound breast cancer images, (b) Ground truth segmented images, segmented results by (c) Method 1, (d) Method 2, (e) Method 3, (f) Method 4, (g) Method 5, (h) Method 6, (i) Method 7 and (j) Method 8.

Table 4
Quantitative evaluations for Segmentation algorithms.

	Algorithm / performance metrics	JI	DS	AD
Sample I	*K*-means	0.6071	0.6769	1.617
	FCM	0.8982	0.8510	1.5103
	GKFCM	0.8772	0.8899	1.439
	NLM	0.7572	0.6453	3.1970
	Graph-based	0.8840	0.8512	1.6170
	watershed	0.6215	0.6351	4.6543
	MsGKFCM	**0.9772**	**0.9334**	**0.8302**
Sample II	*K*-means	0.6110	0.6801	1.1815
	FCM	0.6927	0.7231	1.1854
	GKFCM	0.8760	0.8909	1.1630
	NLM	0.7348	0.7656	3.8140
	Graph-based	0.7855	0.8943	1.5103
	watershed	0.6432	0.6876	3.9878
	MsGKFCM	**0.8891**	**0.9345**	**1.1549**
Sample III	*K*-means	0.7258	0.7977	0.8529
	FCM	0.8231	0.8940	0.8828
	GKFCM	0.8471	0.8662	0.6066
	NLM	0.7184	0.7234	3.3773
	Graph-based	0.8437	0.8763	0.9891
	watershed	0.6856	0.7645	3.1234
	MsGKFCM	**0.9430**	**0.9227**	**0.5781**
Sample IV	*K*-means	0.8253	0.7645	1.6282
	FCM	0.8113	0.8761	0.9333
	GKFCM	0.8581	0.9011	0.8427
	NLM	0.6563	0.6876	3.2976
	Graph-based	0.8920	0.8756	1.7854
	watershed	0.6787	0.6598	3.7865
	MsGKFCM	**0.8920**	**0.9212**	**0.7442**
Sample V	*K*-means	0.7332	0.7998	1.339
	FCM	0.8588	0.7952	1.1454
	GKFCM	0.9026	0.9233	0.69265
	NLM	0.7492	0.7673	3.6867
	Graph-based	0.8531	0.8543	0.8756
	watershed	0.7897	0.7231	2.7853
	MsGKFCM	**0.9558**	**0.9543**	**0.5921**
Mean ± STD	K-means	0.700 ± 0.092	0.743 ± 0.061	1.256 ± 0.353
	FCM	0.816 ± 0.077	0.827 ± 0.069	1.105 ± 0.253
	GKFCM	0.872 ± 0.021	0.894 ± 0.020	0.948 ± 0.346
	NLM	0.723 ± 0.040	0.717 ± 0.052	3.474 ± 0.263
	Graph-based	0.851 ± 0.042	0.870 ± 0.017	1.355 ± 0.400
	watershed	0.683 ± 0.064	0.694 ± 0.051	3.667 ± 0.735
	MsGKFCM	**0.931 ± 0.039**	**0.933 ± 0.013**	**0.779 ± 0.234**

Table 5
Shape similarity using Hausdroff difference (pixels).

Algorithm	Sample I	Sample II	Sample III	Sample IV	Sample V	Mean ± STD
ACM	4.4742	4.6230	3.4242	2.8525	3.8427	3.843 ± 0.735
GVF	3.2498	6.4430	4.8546	3.1212	3.3861	4.210 ± 1.430
VFC	2.4542	2.3832	1.8515	3.1014	2.9561	2.569 ± 0.527
MsVFC	**1.5260**	**2.2256**	**1.3902**	**2.1404**	**1.4828**	**1.753 ± 0.396**

Table 6
Accuracy (%) for segmentation algorithms.

Algorithm	Accuracy (Mean ± STD)	*F*-score (Mean ± STD)	Specificity (Mean ± STD)	Precision (Mean ± STD)	Recall (Mean ± STD)
K-means	84.5180 ± 0.0360	73.3685 ± 0.0656	14.8767 ± 0.1464	80.7588 ± 0.0271	77.2754 ± 0.0439
FCM	89.4515 ± 0.0329	88.0660 ± 0.0261	19.8945 ± 0.0533	83.1513 ± 0.0261	89.5902 ± 0.2476
GKFCM	95.5800 ± 0.0156	90.2427 ± 0.0576	14.4700 ± 0.0439	83.9596 ± 0.0239	93.4004 ± 0.0533
NLM	82.2310 ± 0.0498	87.1780 ± 0.0316	16.3487 ± 0.1316	85.3710 ± 0.0271	88.1129 ± 0.0436
Graph-based	89.7840 ± 0.0460	88.5060 ± 0.0545	13.4890 ± 0.1316	87.3670 ± 0.0316	89.5038 ± 0.0394
watershed	60.1670 ± 0.0846	62.5670 ± 0.0532	16.7340 ± 0.1316	66.4650 ± 0.0522	68.4175 ± 0.0316
MsGKFCM	**97.3158 ± 0.0409**	**92.310 ± 0.0246**	**12.7777 ± 0.0246**	**86.4956 ± 0.0244**	**94.3291 ± 0.0385**

Table 7 shows the statistical test result of one-way Analysis of Variance (ANOVA) test between segmented breast US lesion area generate by proposed method (MsGKFCM) and Ground truth that manually annoted by expert. One-way ANOVA test has been performed to statistically assess the superiority of the method. The statistical test measures the stability and reliability of the system. A statistical test will rejects or accept the null hypothesis. The null hypothesis is normally an assumption that the two quantities are associated with each other. In this study, the statistical analysis is performed using SPSS software with 0.05 significance level. In Table 7, DF indicates degrees of freedom, SS sum of squares and MS mean square. The results of ANOVA test shows the *F*-value (0.0124) is less than *F*-critical (3.8786) and *P*-value (0.9113) is above 0.05.

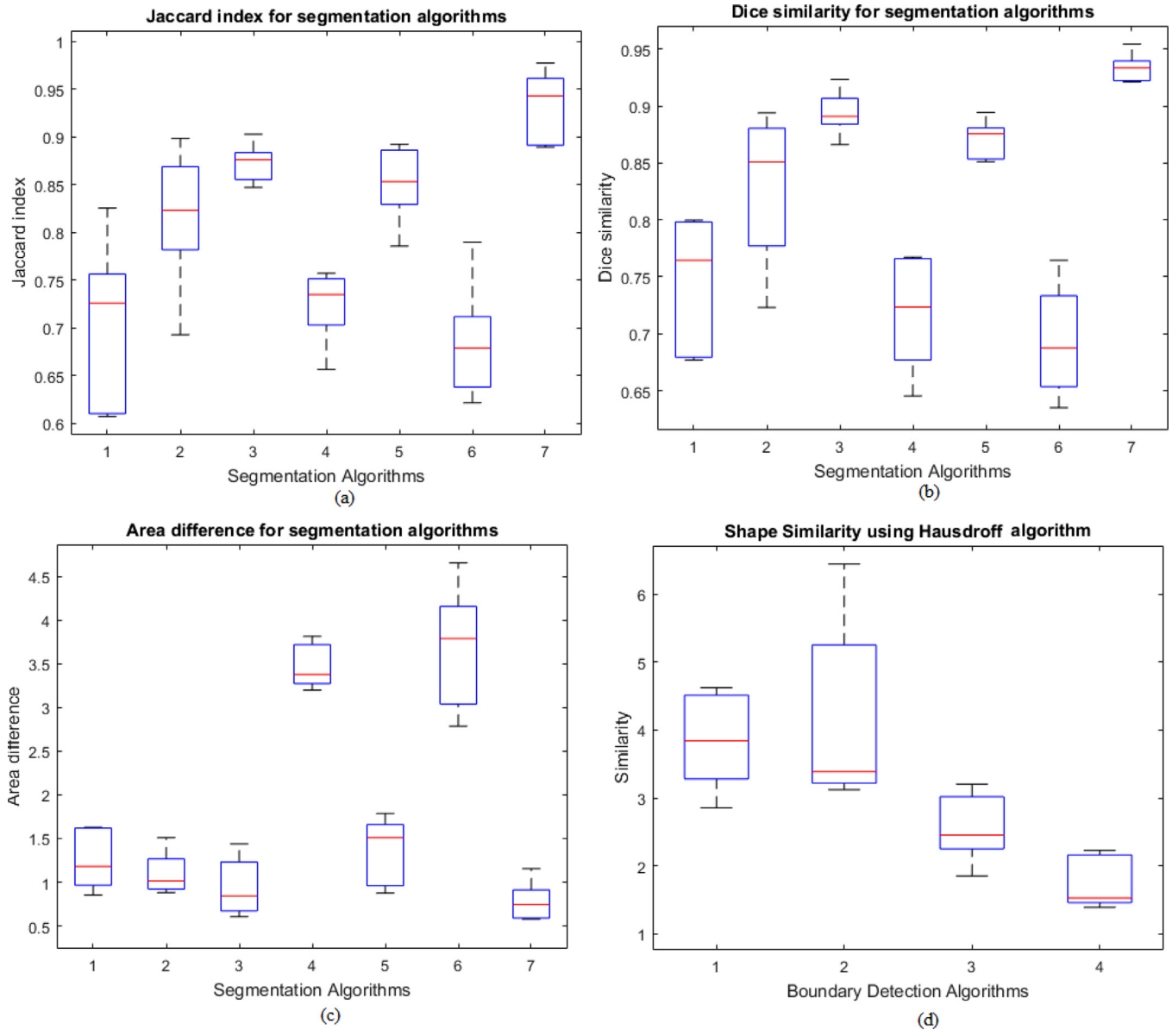

Fig. 4. Box plot of the (a) JI for segmentation algorithms,(b) DS for segmentation algorithms,(c) Difference in area for segmentation algorithms and (d) HD for boundary detection algorithms.

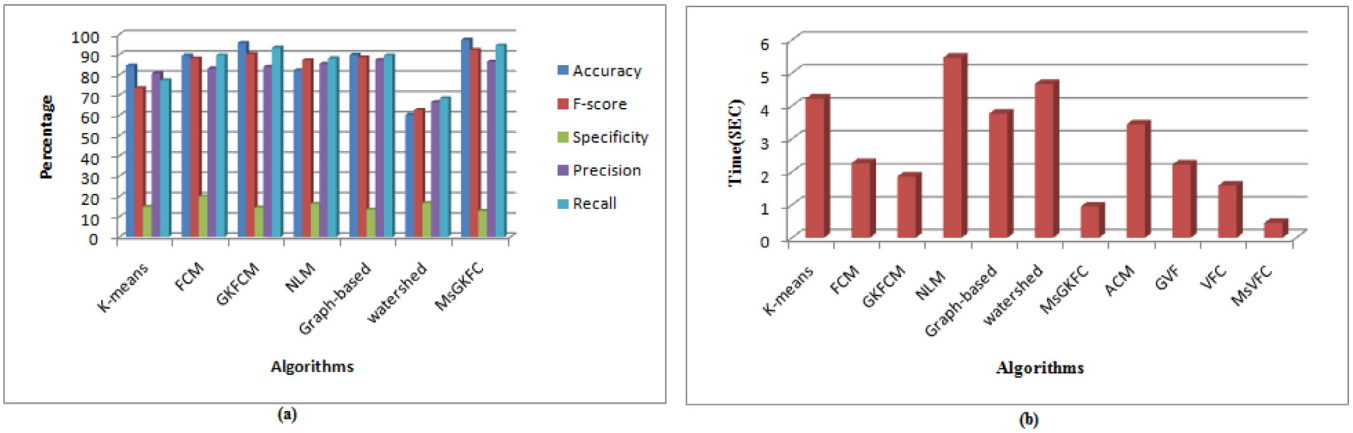

Fig. 5. Bar chart of (a)accuracy and (b) computational time for different algorithms.

Table 7
One-way ANOVA test between area generate by MsGKFCM and Ground truth method.

Source of variation	SS	df	MS	*F*-value	*P*-value	F-critical
Between Groups	0.1742	1	0.1742	0.0124	0.9113	3.8786
Within Groups	3533.168	252	14.0205			
Total	3533.342	253				

Table 8
Computational time of Segmentation and Boundary detection algorithm.

Algorithm	Time (s)	Algorithm	Time (s)
K-means	4.224	**MsGKFCM**	**0.949**
FCM	2.267	ACM	3.441
GKFCM	1.859	GVF	2.221
NLM	5.463	VFC	1.585
Graph-based	3.767	**MsVFC**	**0.449**
watershed	4.665		

The computational time for all the segmentation as well as boundary detection techniques is computed. For such relative analysis, the averaged computational time in seconds taken by the individual methods is shown in Table 8. It can be observed from the table that the proposed method is computationally faster than the other existing segmentation methods and boundary detection methods due to Chen and Zhang (2004) this study, eliminated the term R_i to overcome the limitation of MsFCM (all the mathematical description described in sections 2 and 3.3).

The box plots of all quantitative results of the proposed and state-of-the-art segmentation algorithm are shown in Fig. 4. In each box plot, the top and bottom of each rectangular box indicate the 25th and 75th percentile, respectively, with the median shown inside the box. It is observed from Fig. 4 that the median of the JI, DS, ACC and AD values gained by the proposed method are highest and lowest, respectively. It also indicates the advantage of the proposed method compared to others in terms of the successful extraction of the region of interest. Fig. 4(a) represents the box plot of JI for segmentation algorithm, the box plot of the DS are illustrated in Fig. 4(b) and (c) shows the difference in area for segmentation algorithm and HD for segmentation algorithm is represented in Fig. 4(d). In Fig. 4(a) and (b) the top rectangular box indicates that the proposed method is more closer to the ground truth than others benchmark techniques. In Fig. 4(c) and (d) the bottom box indicate that there are less area difference and less HD than others. Finally the bar chart of accuracy and computational time for different algorithms illustrated in Fig. 5(a) and (b) respectively.

The strengths and weaknesses of the proposed approach are summarized as follows:

1. It updates the membership of each pixel in a coarse-to-fine fashion using multi-scale.
2. The multi scale approach can successfully improve the clustering speed and can avoid trapping into local solutions.
3. The parameter σ in the other existing methods are priori assigned by users which is significantly affect the clustering results. But in the proposed method the parameter σ is estimated by Eq. (27).
4. The proposed approach is computationally faster than the other existing methods.
5. The parameters α and β affects the clustering results (Yang & Tsai, 2008).

5. Conclusion

In this paper, we have presented a novel segmentation technique which automatically segments the breast US images. This paper overcomes the shortcomings of GKFCM, MsGKFCM and MsVFC method by incorporating multiple scales for construction of crude image to fine using a new objective function. It eliminates the necessity of manual tracing and reduces the computation time also. We conclude that the proposed method is more accurate and performs more effective compared to the benchmark algorithms. A series of experimental results show the capability and efficiency of the proposed approach.

In future, the proposed technique can be improved in several ways such as: (1) Improved inter-and intra-observer variability's and ground truth designs. In terms of inter-and intra-observer variability, multiple breast radiologists can give the scores on the malignant and benign lesions which can then be used as ground truth labels, (2) The proposed method can be evaluated on larger data set, (3) Expert opinion will be accessed to improve the results, (4) This study concentrated on 2-D BUS images. Future study can be focused on segmentation of breast masses using 3-D BUS images.

Acknowledgements

We are thankful to Dr. Satyabhuwan Singh Netam (Associate Professor and Head of Department) and Dr. Bhagyashri, Dr. Bhimrao Ambedkar Memorial Government Medical Hospital, Raipur, Chhattisgarh, India, for providing us the data. We are also thankful to ethical committee NIT Raipur for providing ethical permission.

References

Ahmed, M. N., Yamany, S. M., Mohamed, N., Farag, A. A., & Moriarty, T. (2002). A modified fuzzy c-means algorithm for bias field estimation and segmentation of mri data. *IEEE Transactions on Medical Imaging, 21*, 193–199. doi:10.1109/42.996338.

Avendi, M., Kheradvar, A., & Jafarkhani, H. (2016). A combined deep learning and deformable-model approach to fully automatic segmentation of the left ventricle in cardiac mri. *Medical Image Analysis, 30*, 108–119. doi:10.1016/j.media.2016.01.005.

Bezdek, J. C. (1981). Pattern recognition with fuzzy objective function algorithms. *Plenum Press*. doi:10.1007/978-1-4757-0450-1.

Bikesh, K. S., Kesari, V., Lipismita, P., & Thoke, A. S. (2017). Integrating radiologist feedback with computer aided diagnostic systems for breast cancer risk prediction in ultrasonic images: An experimental investigation in machine learning paradigm. *Expert Systems with Applications, 90*(3), 209–223.

Bo, L., HD, C., Jianhua, H., Jiawei, T., Xianglong, T., & Jiafeng, L. (2010). Probability density difference-based active contour for ultrasound image segmentation. *Pattern Recognition, 43*(6), 2028–2042.

Cahan, A., & James, J. C. (2017). A learning health care system using computer-aided diagnosis. *Journal of Medical Internet Research, 19*(3). xxx–xxx

Chen, S., & Zhang, D. (2004). Robust image segmentation using fcm with spatial constrains based on new kernel-induced distance measure. *IEEE Trans Systems Man Cybernet, 34*, 1907–1916. doi:10.1109/TSMCB.2004.831165.

Chen, Y., Yin, R., Flynn, P., & Broschat, S. (2003). Aggressive region growing for speckle reduction in ultrasound images. *Pattern Recognition Letters, 24*, 677–691. doi:10.1016/S0167-8655(02)00174-5.

Chunming, L., Chenyang, X., Changfeng, G., & Fox, M. (2005). Level set evolution with-out re-initialization: A new variational formulation. In *Proceedings of the IEEE conference on computer vision and pattern recognition* (pp. 430–436). doi:10.1109/CVPR.2005.213.

Chunming, L., Chenyang, X., Changfeng, G., & Fox, M. (2010). Distance regularized level set evolution and its application to image segmentation. *IEEE Trans. Image Process, 19*, 3243–3254. doi:10.1109/TIP.2010.2069690.

Chunming, L., Chiu-Yen, K., Gore, J., & Zhaohua, D. (2007). Implicit active contours driven by local binary fitting energy. In *Proceeding of IEEE conference on computer vision and pattern recognition* (pp. 1–7). doi:10.1109/CVPR.2007.383014.

Cohen, L. D. (1991). On active contour models and balloons. *Computer Vision, Graphics, and Image Processing: Image Understanding, 53*, 211–218. doi:10.1016/1049-9660(91)90028-N.

Cohen, L. D., & Cohen, I. (1993). Finite-element methods for active contour models and balloons for 2-d and 3-d images. *IEEE Transactions on Pattern Analysis and Machine Intelligence, 15*, 1131–1147. doi:10.1109/34.244675.

Dora, L., Agrawal, S., Panda, R., & Abraham, A. (2017). Optimal breast cancer classification using gaussnewton representation based algorithm. *Expert Systems With Applications, 85*, 134–145. doi:10.1016/j.eswa.2017.05.035.

Dunn, J. C. (1973). A fuzzy relative of the isodata process and its use in detecting compact well-separated clusters. *Journal of Cybernetics, 3*, 32–57. doi:10.1080/01969727308546046.

Fenster, A., & Chiu, B. (2005). Evaluation of segmentation algorithms for medical imaging. *Engineering in Medicine and Biology Society, 2005. 27th Annual International Conference of the IEEE-EMBS* (pp. 7186–7189). IEEE.

Gao, G., Wen, C., Wang, H., & Xu, L. (2017). Fast multiregion image segmentation using statistical sctive contours. *IEEE Signal Processing Letters, 24*(4), 417–421. doi:10.1109/LSP.2017.2664659.

Gerard, P., Joan, M., Robert, M., Sergi, G., & Alison, N. J. (2016). Breast-lesion segmentation combining b-mode and elastography ultrasound. *Ultrasonic Imaging, 38*(3), 209–224.

Gerard, P., Robert, M., Sergi, G., Melcior, S., & Joan, M. (2014). Computerized detection of breast lesions using deformable part models in ultrasound images. *Ultrasound in Medicine and Biology, 40*(9), 2252–2264.

Gupta, D., Anand, R., & Tyagi, B. (2015). A hybrid segmentation method based on gaussian kernel fuzzy clustering and region based active contour model for ultrasound medical images. *Elsevier, Biomedical Signal Processing and Control, 16*, 98–112. doi:10.1016/j.bspc.2014.09.013.

Haoyang, S., Yingtao, Z., Min, X., HD, C., Fei, X., & Jianrui, D. (2015). *A saliency model for automated tumor detection in breast ultrasound images* (pp. 1424–1428).

Joo, S., Yang, Y. S., Moon, W. K., & Kim, H. C. (2004). Computer-aided diagnosis of solid breast nodules: Use of an artificial neural network based on multiple sonographic features. *IEEE Transactions on Medical Imaging, 23*(10), 1292–1300. doi:10.1109/TMI.2004.834617.

Juan, S., HD, C., & Yuxuan, W. (2012). A novel segmentation method for breast ultrasound images based on neutrosophic l-means clustering. *Medical Physics, 39*(9), 5669–5682.

Kass, M., Witkin, A., & Terzopoulos, D. (1988). Snakes active contour models. *International Journal of Computer Vision, 1*, 321–331. doi:10.1007/BF00133570.

Kyung, M. W., Chung-Ming, L., Rong-Tai, C., Yi-Wei, S., Min, C. J., Chiun-Sheng, H., et al. (2014). Tumor detection in automated breast ultrasound images using quantitative tissue clustering. *Medical Physics, 41*(4).

Lal, M., Kaur, L., & Gupta, S. (2018). Automatic segmentation of tumors in B-Mode breast ultrasound images using information gain based neutrosophic clustering. *Journal of X-ray science and technology, 26*(2), 209–225.

Laursen, L. (2016). *Doctors still struggle to make the most of computer-aided diagnosis*. IEEE spectrum.

Li, B., & Acton, S. T. (2007). Active contour external force using vector field convolution for image segmentation. *IEEE Transactions on Image Processing, 16*(8), 2096–2106. doi:10.1109/TIP.2007.899601.

Lo, C. M., Chen, R. T., Chang, Y. C., Yang, Y. W., Hung, M. J., Huang, C. S., & Chang, R. F. (2014). Multi dimensional tumor detection in automated whole breast ultrasound using topographic watershed. *IEEE Transactions on Medical Imaging, 33*(7), 1503–1511. doi:10.1109/TMI.2014.2315206.

Madabhushi, A., & Metaxas, D. N. (2003). Combining low-, high-level and empirical domain knowledge for automated segmentation of ultrasonic breast lesions. *IEEE Transactions on Medical Imaging, 22*(2), 155–169. doi:10.1109/TMI.2002.808364.

Min, X., Yingtao, Z., HD, C., Fei, X., Boyu, Z., & Jianrui, D. (2017). *Automatic breast ultrasound image segmentation: A survey*. Infinite Study.

Ortiz, A., Górriz, J. M., Ramirez, J., & Salas-Gonzale, D. (2011). MR brain image segmentation by growing hierarchical SOM and probability clustering. *Electronics Letters, 47*(10), 585–586.

Ortiz, A., Górriz, J. M., Ramirez, J., & Salas-Gonzale, D. (2012). Unsupervised neural techniques applied to mr brain image segmentation. *Advances in Artificial Neural Systems*, 1.

Ortiz, A., Górriz, J. M., Ramirez, J., & Salas-Gonzale, D. (2014). Improving mr brain image segmentation using self-organising maps and entropy-gradient clustering. *Information Sciences, 262*, 117–136.

Panigrahi, L., Verma, K., & Singh, B. K. (2016). An enhancement in automatic seed selection inbreast cancer ultrasound images using texture features. *International conference on advances in computing, communications and informatics (ICACCI)*. doi:10.1109/ICACCI.2016.7732191.

Rastgarpour, M., Shanbehzadeh, J., & Zadeh, H. (2014). A hybrid method based on fuzzy clustering and local region-based level set for segmentation of in homogeneous medical images. *Journal of Medical Systems, 38*(8), 1–15. doi:10.1007/s10916-014-0068-3.

Ray, N., & Acton, S. T. (2004). Motion gradient vector flow: An external force for tracking rolling leukocytes with shape and size constrained active contours. *IEEE Transactions on Medical Imaging, 23*, 1466–1478. doi:10.1109/TMI.2004.835603.

Rogai, F., Manfredi, C., & Bocchi, L. (2016). Metaheuristics for specialization of a segmentation algorithm for ultrasound images. *IEEE Transactions On Evolutionary Computation, 20*(5), 730–741. doi:10.1109/TEVC.2016.2515660.

Ruspini, E. (1969). A new approach to clustering. *Elsevier, Information and Control, 15*, 22–32. doi:10.1016/S0019-9958(69)90591-9.

Sang, Q., Lin, Z., & Acton, S. T. (2016). Learning automata for image segmentation. *Pattern Recognition Letters, 74*, 46–52. doi:10.1016/j.patrec.2015.12.004.

Sassi, O. B., Sellami, L., Slima, M. B., Hamida, A. B., & Chtourou, K. (2014). Multi-slices breast ultrasound lesion segmentation using multi-scale vector field convolution snake. In *1st International conference on advanced technologies for signal and image processing* (pp. 188–192). doi:10.1109/ATSIP.2014.6834604.

Selvan, S., Kavitha, M., Shenbagadevi, S., & Suresh, S. (2010). Feature extraction for characterization of breast lesions in ultrasound echography and elastography. *Journal of Computer Science, 6*(1), 67–74.

Udupa, J., LaBlanc, V., Schmidt, H., Imielinska, C., Saha, P., Grevera, G., et al. (2002). Methodology for evaluating image segmentation algorithms. In *Proceedings of SPIE, medical imaging* (p. 266277). doi:10.1117/12.467166.

Wang, H., & Fei, B. (2009). A modified fuzzy c-means classification method using a multiscale diffusion filtering scheme. *Medical Image Analysis, 13*, 193–202. doi:10.1016/j.media.2008.06.014.

Wang, W., Zhu, L., Qin, J., Chui, Y.-P., Li, B., & Heng, P.-A. (2014). Multi scale geodesic active contours for ultrasound image segmentation using speckle reducing anisotropic diffusion. *Optics and Lasers in Engineering, 54*, 105–116. doi:10.1016/j.optlaseng.2013.10.003.

Xian, M., Zhang, Y., Cheng, H. D., Xu, F., Zhang, B., & Ding, J. (2018). Automatic breast ultrasound image segmentation: A survey. *Pattern Recognition, 79*(10), 340–355.

Xu, C., & Prince, J. L. (1997). Gradient vector flow: A new external force for snakes. In *Proceedings of IEE conference on computer vision* (pp. 66–71). doi:10.1109/CVPR.1997.609299.

Xu, C., & Prince, J. L. (1998). Snakes, shapes, and gradient vector flow. *IEEE Transactions on Image Processing, 7*, 359–369. doi:10.1109/83.661186.

Yang, C., & Acton, S. T. (2012). External forces for active contours via multi-scale vector field convolution. *IEEE International Conference on Image Processing*. doi:10.1109/ICIP.2012.6467423.

Yang, M., & Tsai, H. (2008). A gaussian kernel-based fuzzy c-means algorithm with a spatial bias correction. *Pattern Recognition Lett., 29*(12), 1713–1725. doi:10.1016/j.patrec.2008.04.016.

Yu, Y., & Acton, S. T. (2002). Speckle reducing anisotropic diffusion. *IEEE Transactions on Image Processing, 11*(11), 1260–1270. doi:10.1109/TIP.2002.804276.

Yuan, J. (2012). Active contour driven by region-scalable fitting and local bhattacharyya distance energies for ultrasound image segmentation. *IET Image Process, 6*(8), 1075–1083. doi:10.1049/iet-ipr.2012.0120.

Yuan, J. (2013). Active contour driven by local divergence energies for ultrasound image segmentation. *IET Image Process, 7*(3), 252–259. doi:10.1049/iet-ipr.2012.0461.

Zhang, Q., Huang, C., Li, C., Yang, L., & Wang, W. (2012). Ultrasound image segmentation based on multi-scale fuzzy c-means and particle swarm optimization. *Information Science and Control Engineering*. doi:10.1049/cp.2012.2294.

Lipismita Panigrahi proposed a novel algorithm clustering algorithm called MsGK-FCM. The objective function of the conventional GKFCM is modified for multi-scale thus the result from a coarse scale supervises the cluster of the next fine scale.

Bikesh Kumar Singh performed noise reduction technique, i.e. speckle reducing anisotropic diffusion (SRAD) by building a multi-scale demonstration for each image where the noise is regularly reduced as the scale increases.

Kesari Verma performed the algorithm evaluation part with Jaccard Index, Dice imilarity, Shape similarity, Hausdroff difference, Area difference, Accuracy, F-measure and analysis of variance (ANOVA) test.